

DILUTE GAS-SOLID FLOW IN MILL-DUCT BIFURCATION: CFD SIMULATION AND EXPERIMENTAL VALIDATION

Benny KUAN¹, William YANG¹, Chris SOLNORDAI² and Phil SCHWARZ²

¹ CRC – Clean Power from Lignite, Mulgrave, Victoria 3170, AUSTRALIA

² CSIRO Minerals, Clayton, Victoria 3169, AUSTRALIA

ABSTRACT

Computational Fluid Dynamics (CFD) simulations and experimental measurements have been performed to study dilute gas-solid flow entering a bifurcation duct downstream of a curved 90° bend. The inlet to the model bifurcation duct is square-sectioned and has a hydraulic diameter of 250 mm. The model is a scaled replica of a real bifurcation duct which is being used to split the flow of pulverised coal particles in a Lignite-fired power station. Both computer simulation and laboratory experiment have been carried out at a bulk gas velocity of 11 m/s and with spherical glass particles having a volume-weighted mean diameter of 77 μm. The numerical studies show significant flow instabilities within the bifurcated ducts. The averaged gas and solids flow properties are measured using Laser-Doppler Anemometry (LDA) and they have been applied to validate the numerical predictions.

NOMENCLATURE

C	model constants
C_D	drag coefficient
D	hydraulic diameter of the duct
d_p	particle diameter
F	force vector
f_D	Schiller-Naumann drag correlation
G	turbulence production
g	gravity vector
k	turbulence kinetic energy
L	solids mass loading = \dot{m}_p / \dot{m}_f
\dot{m}	mass flow rate
R	duct turning radius
Re	duct Reynolds number
s, r*	curvilinear coordinate system on the duct plane of symmetry; r* = 0 at outer wall; r* = 1 at inner wall
U	mean gas velocity vector
U, V	mean longitudinal and transverse velocity components
U_b	bulk gas velocity
U_T	particle terminal velocity
u	instantaneous velocity vector
u'	Fluctuating velocity vector
u', v'	fluctuating longitudinal and transverse velocity components

Greek letters

δ_{ij} Kronecker delta

ε	eddy dissipation rate
μ	gas dynamic viscosity
ν	gas kinematic viscosity
θ	duct turning angle
ρ	density
τ	time scale

Subscripts

A	added mass
D	drag
f	fluid
g	gravity
i, j, k	tensor index
p	particle
pg	pressure gradient
sl	slip-shear lift

INTRODUCTION

In coal-fired power plants that rely on a continuous supply of coal for electricity generation, the coal needs to be first pulverised in coal mills, and then pneumatically transported and distributed to a large number of burners that are positioned around the furnaces. In order to avoid the formation of NO_x as well as lower the level of unburned carbon, it is essential to maintain a homogeneous injection of the coal-air mixture into the furnaces. This requires a good control over the supply of the pulverised fuel (PF) to individual burners.

In reality, such a condition rarely exists. The pneumatic pipelines that deliver PF from the mills to the burners form a complex pipe network consisting of numerous bends and junctions. As the PF flow passes through a bend, each coal particle experiences centrifugal action due to its own inertia and a coal-dense mixture known as a rope is formed downstream from the bend. Thus, the PF concentration becomes non-uniform over the pipe cross-section after the bends. This, subsequently, causes an uneven split of the PF flow at the bifurcation which acts to distribute the coal-air mixture to downstream burners.

In order to address this problem, Griddings et al. (2004) have conducted both experimental and numerical investigations in a model pipe network that consists of either a bifurcation or trifurcation at duct Reynolds number $Re \sim 1.0 \times 10^5$. In their experiment, split of the mass flow at the bifurcation varied between 42%:58% and 49%:51% depending on the solids loading. In the trifurcation, the measured split ranged from 16%:26%:58% to 17%:38%:45%. The position of the

Results presented in this paper were obtained under a benchmark experimental condition where the bulk gas velocity, U_b , was set to 11m/s leading to a duct Reynolds number (based on the bulk velocity, duct hydraulic diameter and air kinematic viscosity) of 1.8×10^5 .

Particle size distribution of the glass spheres was determined from a wet analysis in a Malvern particle sizer and it is given in Fig. 2. The volume-weighted mean diameter of the particles as measured by the particle sizer is 77 μm . The glass spheres were released into the flow field to achieve the tested feed rate of 9 kg/hr which gives a gas-solid mass loading of 0.297%. At such a low solids mass loading, one can reasonably assume a negligible transfer of particle momentum to the carrier-phase, i.e. one-way coupling.

Yang and Kuan (2006) have provided further detail on the laboratory setup adopted in the current study.

MODEL DESCRIPTION

Gas-phase

Unsteady, isothermal gas flow properties and turbulence quantities are calculated numerically by solving a set of governing partial differential equations (PDE) using the commercial CFD software ANSYS CFX-10.0. The set of PDEs solved includes Reynolds-averaged Navier-Stokes equations, transport equations for Reynolds stresses (Speziale et al., 1991) and turbulent dissipation rate ϵ .

Particle-phase

Instantaneous positions and velocities of the dispersed phase are solved through a Lagrangian particle tracking method. Motion of individual particles suspended in a continuous fluid is determined by numerically integrating the equations of motion for the dispersed phase in a fluid flow. The equation of particle motion may be expressed as

$$m_p d\mathbf{u}_p / dt = \mathbf{F}_D + \mathbf{F}_g + \mathbf{F}_{pg} + \mathbf{F}_A + \mathbf{F}_{sl} \quad (1)$$

$$d\mathbf{x}_p / dt = \mathbf{u}_p \quad (2)$$

where m_p is particle mass and subscripts D, g, pg, A and sl respectively denote force components arising from drag, gravity, flow pressure gradient, added mass effect and slip-shear lift.

The drag force is calculated from

$$\mathbf{F}_D = m_p (\mathbf{u}_f - \mathbf{u}_p) / \tau_r \quad (3)$$

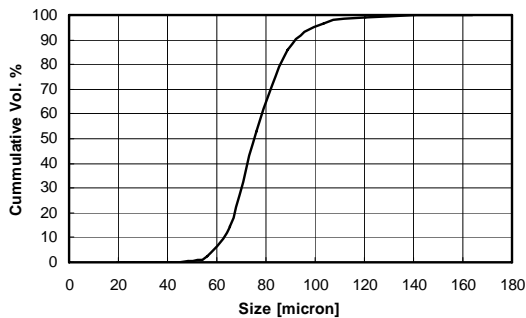


Figure 2. Measured cumulative particle size distribution

with $\mathbf{u}_f = \mathbf{U} + \mathbf{u}'$ and particle relaxation time τ_r defined

$$\text{by } \tau_r = \rho_p d_p^2 / 18 \mu f_D \quad (4)$$

where f_D is Schiller-Naumann drag correlation for a sphere. The force components due to gravity \mathbf{F}_g , added mass \mathbf{F}_A , and shear-slip lift \mathbf{F}_{sl} are given in Kuan et al. (2006).

The present simulation adopts a modified version of the particle-wall interaction model of Matsumoto and Saito (1970). The base-case model allows the particles to either slide along the wall surface when the angle of incidence is small, or rebound away from the wall after impact. However, it is based on the assumption of a constant restitution coefficient and dynamic friction, both of which are sensitive to a range of parameters, such as incidence angle and wall material, as found in published experimental investigations of Frank et al. (1993), Sommerfeld and Huber (1999).

For the present numerical calculation which involves collisions between the glass spheres and the Perspex duct walls, impact test data for glass beads on Plexiglass plates are utilized to characterize the particle-wall interaction (Sommerfeld and Huber, 1999). Details of the particle-wall interaction model considered are available in Kuan et al. (2006).

NUMERICAL PROCEDURE

The duct interior including the Y-junction is mapped to a curvilinear grid system of more than 1,300,000 hexahedral cells. The partial differential equations are discretised following a finite volume approach. The advection terms were approximated using a scheme developed by Barth and Jespersen (1989) which is more than first-order accurate at mesh discontinuities and provides higher-order accuracy for smoothly varying meshes. The discretised governing equations for the gas phase are then solved using the commercial package CFX-10.0.

The current simulation utilises a set of fully-turbulent inflow conditions for the gas phase and zero-slip condition (i.e. $\mathbf{u}_p = \mathbf{u}_f$) for the particles. Mass conservation and zero-gradient condition have been imposed at the outflow boundary which is located at 0.5 m downstream of the Y-junction. Transient calculations have been performed at time steps of 0.0005 s over a 0.92 s period which is more than twice the gas transit time through the duct.

In the simulation, the measured particle size distribution is represented by 13 characteristic particle size fractions. We have applied 8000 particle tracks to represent a group of 'real' particles of the same size in each size fraction. Overall, there are a total of 104000 particle tracks in the simulation. The resulting particle statistics have been averaged following the approach of Kuan et al. (2006).

RESULTS

Flow before the Split

The predicted gas velocity vectors tangential to duct cross sections at 0D, 0.5D and 1D downstream of the bend are presented in Fig. 3. The bend imparts a significant centrifugal motion on the turning gas flow such that by Sta. A, the core gas flow at the duct centre is moving

strongly towards the outer wall ($r^* = 0$), causing the gas at the side walls to circulate.

Measured and predicted mean vertical gas velocities on the symmetry planes of these three cross sections are compared in Fig. 4. All data are normalised by U_b and plotted against a normalised distance r^* which is 0 at the outer wall and 1 at the inner wall. In the vertical duct section downstream of the bend, there is a considerable scatter (instability) in the measured mean gas velocities at $r^* > 0.2$. This is largely due to the presence of wakes at trailing edges of the turning vanes. The unsteady simulation also captured this phenomenon but the level of flow instability is much lower as seen from the oscillations in the predicted gas velocity profile (Fig. 4a). The oscillations, however, have disappeared by 0.5D downstream of the bend (Fig. 4b).

While the scatter in the measured data is still clearly visible by 1D downstream of the bend (Fig. 4c), the data indicates a more uniform gas velocity distribution as compared to the predicted trend. This implies that the laboratory flow remains attached to the inner duct wall following the bend while the predicted flow has separated from the inner wall.

Following the statistical averaging process of Kuan et al. (2006), the mean particle velocity profiles are compared against the measured distributions. In general, the measured particle velocity profiles closely follow their gas-phase counterparts, except in the $r^* < 0.2$ layer. This corresponds to the region where frequent particle-wall collisions occur and thus the particles are lagging the gas by a large margin.

It is interesting to note that the measured particle velocity profile follows the same oscillatory pattern as seen in the gas data. It appears that the particles which lose some of their momentum during collisions with the vane surfaces have no major effect on the particle velocities measured at and downstream of the bend exit. This trend, however, is not observed in the predicted particle velocity profiles. The particles in the simulation possess a much lower vertical velocity within a large portion of the bend exit than these in the laboratory flow. This is largely attributable to particle-wall collisions which took place between the turning vanes. At the bend exit, the simulation also suggests a small pocket of two-phase flow having negligible slip at $r^* > 0.8$. This corresponds to a strong presence of fine particles in the near-wall region ($r^* \sim 1.0$). As the coarse particles approach and centrifuge onto the outer wall downstream of the bend, the size of the low slip region increases as seen in Fig. 4.

Flow in the Lower-leg Duct

Flow instability has disappeared by the time the laboratory flow enters the vertical duct section leading to the lower-leg branch of the bifurcation (Fig. 5). All measured velocity profiles display a peak at $r^* = 0.6$ and a flatter distribution at $r^* < 0.4$. This suggests a steady evolution of the turbulent flow structure up to the bifurcation. Near the inner wall ($r^* = 1.0$), the measured profiles indicate a gradual increase in the mean gas velocity.

The predicted profiles display a similar tendency, namely,

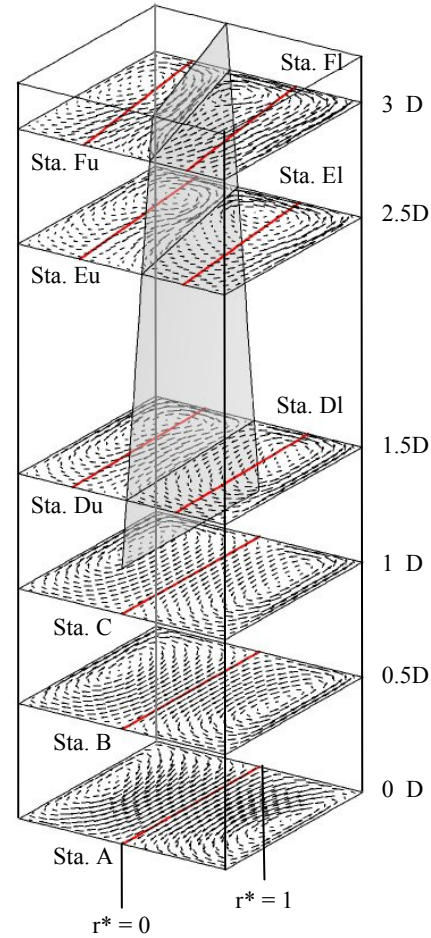


Figure 3. Predicted gas velocity vectors at selected cross sections downstream of the bend

a linear distribution towards the outer wall and flow acceleration near the inner-wall. However, there is no sign of a high-velocity core at $r^* = 0.6$ in the predicted flow field as seen in the measured profiles. Instead, the predicted gas velocity falls to a local minimum of $0.8U_b$ at $r^* = 0.8$. With reference to the predicted velocity vectors at Sta. DI, EI and FI in Fig. 3, this corresponds to the centre of one of the counter-rotating vortex pair. The large discrepancy between the two profiles is thus a result of the model not being able to correctly predict the size and location of this counter-rotating vortex pair which has been positively identified in the experiment by flow visualisation.

Both the prediction and the measurement show considerable gas-particle slip within a narrow layer ($r^* < 0.2$) next to the outer wall as the bulk of the particulate flow continues to centrifuge onto the outer duct wall.

Flow in the Upper-leg Duct

As compared to the data for the lower-leg side of the vertical duct, measured gas velocities in the upper-leg bifurcation duct display distinctly different characteristics (Fig. 6). The peak in the measured velocity profile gradually moves towards the outer wall in the downstream direction. This trend has been qualitatively reproduced in the prediction. The prediction also indicates that the particles are lagging the gas phase by as much as $0.24U_b$

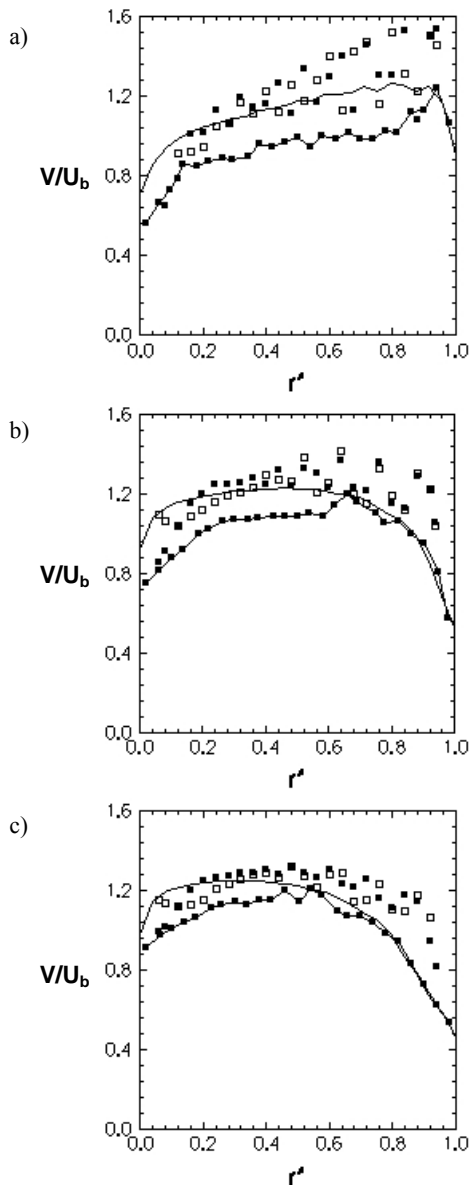


Figure 4. Centreline vertical velocity profiles immediately downstream of the bend a) Sta. A; b) Sta. B; c) Sta. C (\square gas data; \blacksquare particle data; — gas prediction; —■— particle prediction)

within at $r^* < 0.4D$ and this agrees well with the measured trend.

The observed difference between the measured flow properties at either side of the flap is primarily due to the positioning of the flap which respectively provides a narrower passage for the upper-leg and lower-leg flow near the inner and outer wall. This indirectly sets up pressure gradients between the inner and outer duct walls in each duct branch, forcing the gas flow in the lower-leg duct to move towards the inner wall as seen in Fig. 5 and the gas flow in the upper-leg duct towards the outer wall (see Fig. 6). The gas flow in the simulation, by contrast, is not as sensitive to the local pressure gradient across the flow direction. The calculation thus suggests a similar flow structure in the upper- and lower- leg duct downstream of the split (Fig. 5 c.f. Fig. 6).

Predicted Distribution of the Solids

Over the period within which the unsteady flow is calculated, flow instability inside the bifurcation exerts no appreciable influence on the split of the gas and particle flow, which takes place at 2D upstream from the base of the bifurcation. The time-averaged distribution of the predicted gas flow entering the bifurcation ducts is 49.3%: 50.7% (upper-leg: lower-leg). The slight bias is largely the result of flow unsteadiness arising from the turning vanes. The predicted gas flow distribution is thus expected to approach 50%: 50% as one continues the simulation far beyond 0.9 s.

The calculated solids mass flow through each of the bifurcation ducts also indicates an almost equal split of the particulate material, 49.9% : 50.1% (upper-leg : lower-leg). This is to be expected due to the equal split of the duct cross-section by the flap element upstream of the bifurcation and also the fact that the coarse particles tend to segregate from the gas flow within and downstream of the bend.

CONCLUSION

Both laboratory experiment and numerical simulation have been performed to study dilute gas-solid flow passing through a bifurcation with a flap element fitted at its base to evenly divide the solids flow. Mean gas and particle velocities have been measured using LDA technique and they were applied to validate the CFD solution.

Both the experiment and the calculation suggest that the gas flow immediately downstream of the bend is unsteady. However, the flow unsteadiness is unlikely to affect the split of either gas or solids flow at the bifurcation.

In the vertical duct section leading to the bifurcation, the numerical solution provides a qualitative representation of the gas flow field in either side of the duct. The numerical model is unable to accurately resolve the size and location of the prevailing counter-rotating vortices. This has led to strong discrepancies between the measured and predicted flow properties, which is the same problem that Schneider et al. (2002) experienced in their numerical study.

The predicted distribution of the gas flow at the split is 49.3%: 50.7% (upper-leg: lower-leg) and is expected to approach 50%: 50% as the simulation runs beyond the period solved in this study. The predicted split of the solids flow is 49.9%: 50.1% (upper-leg: lower-leg) and appears to be solely dependent on the geometry of the split.

ACKNOWLEDGEMENTS

The authors gratefully acknowledge the financial and other support received for this research from the Cooperative Research Centre for Clean Power from Lignite, which is established and supported under the Australian Government's Cooperative Research Centres program.

REFERENCES

GRIDDINGS, D., AROUSSI, A., PICKERING, S.J., MOZAFFARI, E., (2004). A ¼ scale test facility for PF transport in power station pipelines, *Fuel*, 83, 2195-2204.

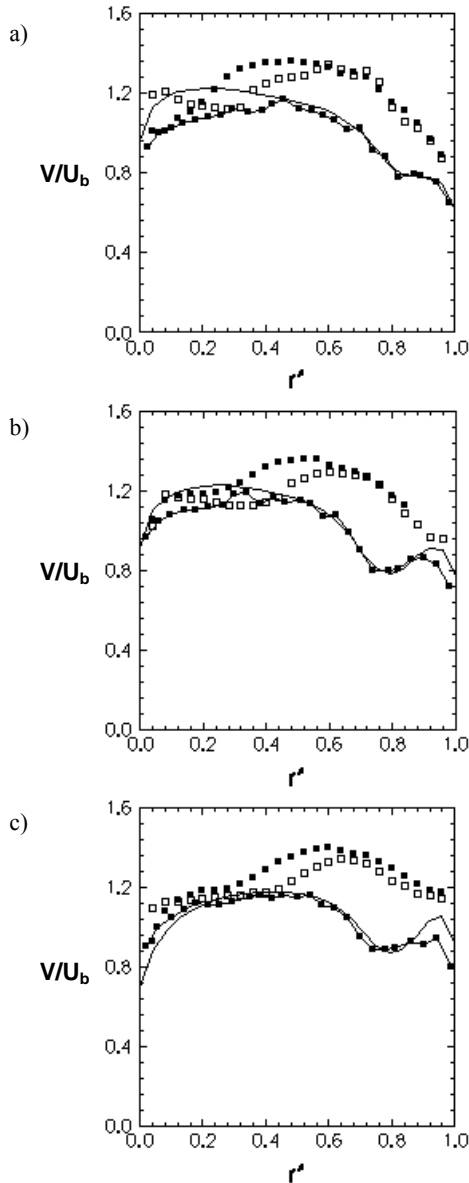


Figure 5. Centreline vertical velocity profiles upstream of the lower-leg bifurcation a) Sta. D1; b) Sta. E1; c) Sta. F1 (\square gas data; \blacksquare particle data; — gas prediction; - - - particle prediction)

SCHNEIDER, H., FRANK, TH., PACHLER, D.K., BERNERT, K., (2002). A numerical study of the gas-particle flow in pipework and flow splitting devices of coal-fired power plant, *Proceedings of the 10th Workshop on Two-Phase Flow Predictions*, 227-236.

YANG, W., KUAN, B., (2006). Experimental investigation of dilute turbulent particulate flow inside a curved 90° bend, *Chemical Engineering Science*, 61, 3593-3601.

SPEZIALE, C.G., SARKAR, S., GATSKI, T.B., (1991). Modelling the pressure-strain correlation of turbulence: an invariant dynamical systems approach, *Journal of Fluid Mechanics*, 227, 245-272.

MATSUMOTO, S., SAITO, S., (1970). Monte Carlo simulation of horizontal pneumatic conveying based on the rough wall model, *Journal of Chemical Engineering of Japan*, 3(1), 223-230.

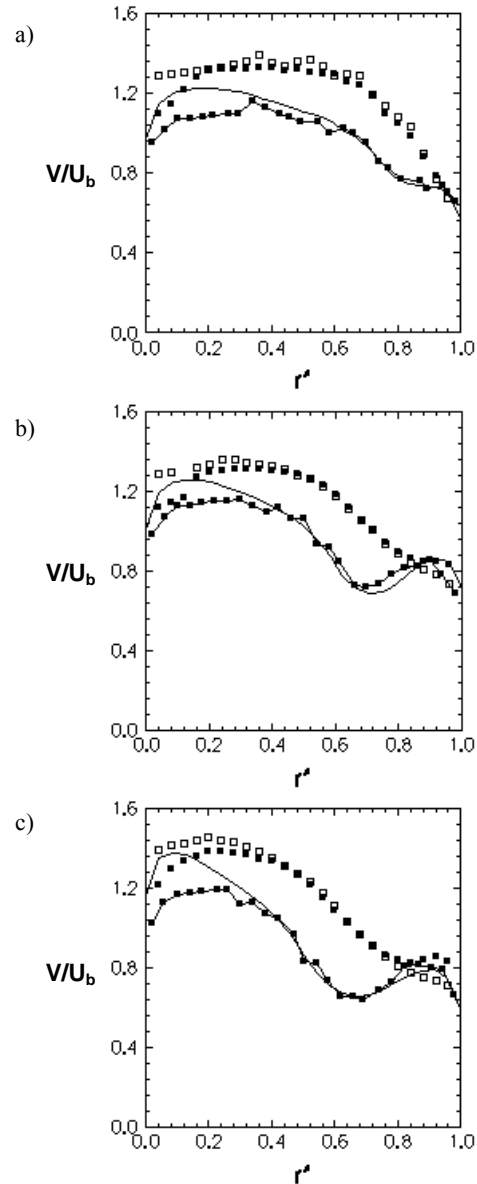


Figure 6. Centreline vertical velocity profiles upstream of the upper-leg bifurcation a) Sta. Du; b) Sta. Eu; c) Sta. Fu (\square gas data; \blacksquare particle data; — gas prediction; - - - particle prediction)

FRANK, TH., SCHADE, F.-P., PETRAK, D., (1993). Numerical simulation and experimental investigation of a gas-solid two-phase flow in a horizontal channel. *International Journal of Multiphase Flow*, 19(1), 187-198.

SOMMERFELD, M., HUBER, N., (1999). Experimental analysis and modelling of particle-wall collisions, *International Journal of Multiphase Flow*, 25, 1457-1489.

BARTH, T.J., JESPERSON, D.C., (1989). The design and application of upwind schemes on unstructured meshes, *AIAA Paper 89-0366*.

KUAN, B., YANG, W., SCHWARZ, M.P., (2006). Dilute gas-solid two-phase flows in a curved 90° duct

bend: CFD simulation with experimental validation,
(submitted to Chemical Engineering Science).